Cent. Eur. J. Phys.
DOI: 10.2478/s11534-013-0286-1

VERSITA

Central European Journal of **Physics**

The mixed spin-1/2 and spin-1 Ising system on a two-layer Bethe lattice

Research Article

Joël Kplé, Gabriel Y. H. Avossevou, Félix Hontinfinde*

Département de Physique (FAST) et Institut de Mathématiques et de Sciences Physiques (IMSP), Université d'Abomey-Calavi, 01 BP 613, Porto-Novo, Benin

Received 26 May 2013; accepted 17 July 2013

Abstract: Two layered magnetic Bethe lattice with varying coordination number q is introduced and numerically studied via exact recursion relations within a pairwise approach. The system is influenced by competing interlayer and intralayer nearest-neighbour (NN) coupling interactions and also by the crystal and external magnetic fields. Cases where both layers are ferromagnetic or one is ferro and the other antiferromagnetic are considered. System configurations' energy calculations are used to devise some ground state phase diagrams that have proven useful for the investigation of the very low temperature behaviour of the model. Analysis of the thermal behaviours of the total magnetization within the model parameters' space yield interesting phase diagrams which display fascinating properties, in particular the presence of tricritical points. Increasing negative values of the crystal field strength stabilizes the disordered paramagnetic phase and sometimes gives rise to wavy transition lines.

PACS (2008): 05.10.-a; 05.20.-y; 05.40.-a; 05.50.+q; 05.70.-a

Keywords: bilayer Bethe lattice • mixed spin-1/2 and spin-1 model • ground states • recursion relations • tricritical and compensation points

1. Introduction

Mixed Ising systems attracted much interest in the last decades from both theoretical and experimental points of view. First, they are among the simplest models that exhibit critical behaviours. In particular, the mixed spin-1/2 and spin-1 got considerable attention because it appears well adapted for the investigation of some special ferrimagnetism [1]. Second, molecular-based magnetic materials and the understanding of their molecular magnetism have become an important focus of scientific and technological interest [2–4].

Various mixed-spin Ising systems can be constructed. The simplest one concerns the mixed spin-1/2 and spin-1 Ising system. It has been studied extensively by a variety of techniques, namely the renormalization group technique [5–8], high-temperature series expansions [9, 10], the free-fermion approximation [11], the Bethe lattice approach [12], the Bethe-Peierls approximation [13–15], the effective-field theory [16–21], the mean-field approximation [22–24], the finite-cluster approximation [25], Monte Carlo simulations [26–28], the mean-field renormalization-group technique [29], the numerical transfer matrix method [27, 28] and the cluster variation method

*E-mail: hontinfinde@yahoo.fr

in pair-approximation [30]. Thus, thin film models that consist of various magnetic layered structures become interesting tools for physicists [31]. Indeed, models of ferromagnetic/ferromagnetic (FM/FM) multilayer with FM interface exchange coupling such as in Co/Cu/Ni [32], FM/antiferromagnetic (AFM) multilayer such as in Fe/NiO [33] and NiO/Co [34], ferrimagnetic/ferrimagnetic superlattices such as in Fe_3O_4/Mn_3O_4 [35] and ferrimagnetic/AFM superlattice such as in Fe_3O_4/CoO [36] have been constructed and thoroughly investigated [37]. Bilayered structures are of particular interest since they display novel properties such as giant magnetoresistance [38, 39], enchanced surface magnetism moment [40, 41], etc. Their study induced technological advances in devices manufacture for information storage and retrieval and also in the synthesis of other magnets of wide applications [42].

The symmetric two-layer Ising model was studied by the corner transfer matrix renormalization group method for critical points and exponents [43] calculations. Monte Carlo simulations were also performed to investigate the Ising model consisting of two FM layers coupled weakly together [44] with different interaction constants. Beyond that, other methods were considered to study the two-layer Ising model: the mean field theory (MFT), the generalized MFT, the scaling approach and the high-temperature series expansions [45]. The critical temperature of this model was precisely calculated by using the transfer matrix mean field approximation [46]. Though each method has it own advantages, they all have limitations in treating thin film systems. Numerical techniques such as the Monte Carlo method can provide very accurate results on the properties of such systems; however, they can only be implemented for relatively small system sizes.

Exact solutions of models that describe such systems are unavailable. One often relies on approximate methods such as the Bethe approximation [47, 48] which yields results that are better than those obtained using the common mean field scheme [49]. Exact calculations are possible when the model is defined on the Bethe lattice [50]. On such a recursive graph, the behaviour of one spin, say the central spin, can lead to the full picture of the whole system.

In the present work, the original one layer Bethe lattice [51, 52] is replaced by two superposed Bethe lattices with the same coordination number q [53–58]. Each of them contains spin-1/2 and spin-1 atoms that are allowed to interact through the bilinear intralayer interactions J_1 (for the upper layer) and J_2 (for the lower layer) between the nearest neighbour (NN) spins of their own layer. Adjacent NN spins of the two layers are tied together via interactions J_3 and J_4 between vertically aligned spin-1/2 and spin-1. These interactions are taken to be either ferromagnetic or antiferromagnetic. The model differs from those developed in Refs. [56, 59] since mixed spins are now considered for each layer.

By means of a pairwise approach [53–58], the underlying recursion relations are solved to calculate the partition function of the system. Using the thermal behaviours of the order parameters and the response functions calculated using the system free energy, the temperature phase diagrams are constructed. They show interesting properties with varying model parameters: reentrance, wavy forms and existence of tricritical points.

In section 2, the model and its formulation are specified. In section 3, the temperature phase diagrams are calculated. The final section is devoted to the conclusion.

2. The model and its formulation

Two identical layers G_1 and G_2 of the Bethe lattices are placed parallel to each other with an exact match, forming the two-layer Bethe lattice [53–58] as seen in Fig.1. Each layer consists of two interpenetrating sublattices containing spin-1/2 atoms (sublattice A) and spin-1 atoms (sublattice B).

The appropriate Hamiltonian of such a system influenced by external magnetic and crystal fields is written as:

$$\begin{aligned} H \;=\; & -J_1 \sum_{<ij>} S_i\sigma_j - J_2 \sum_{<i'j'>} S'_{i'}\sigma'_{j'} - J_3 \sum_{<ii'>} S_i S'_{i'} \\ & -J_4 \sum_{<jj'>} \sigma_j\sigma'_{j'} - D\Big(\sum_j \sigma_j^2 + \sum_{j'} \sigma_{j'}^{\prime 2}\Big) \\ & -h_1\Big(\sum_i S_i + \sum_j \sigma_j\Big) - h_2\Big(\sum_{i'} S'_{i'} + \sum_{j'} \sigma'_{j'}\Big) \end{aligned} \quad (1)$$

where each spin S_i/σ_j located at the neighbouring sites i/j refers to spins in the upper G_1 layer, and is of $\frac{1}{2}/(1)$ type with discrete values $\pm\frac{1}{2}/(\pm 1, 0)$; $S'_{i'}/\sigma'_{j'}$ located at i'/j', refers to corresponding spins in G_2 layer, with the same discrete values as above. The couplings J_1 and J_2 are the intralayer NN bilinear exchange coupling parameters. Analysis of the Hamiltonian will be only performed in the simple case of NN interactions. Thus, the first and the second summations are over all NN sites of G_1 and G_2, respectively. J_3 and J_4 are the interlayer bilinear interactions of adjacent NN spins between the layers, so the third and the fourth summations run over all adjacent neighbouring sites of G_1 and G_2. D is the crystal field interaction strength; two external magnetic fields h_1 and h_2 act on the system.

We exactly calculated the partition function of the system using the recursion relations in a pairwise approach [53,

54, 56–58]. The name "pairwise approach" is used since we form a pair by taking the adjacent NN spins from each layer, then one moves from the root to the boundary sites by considering all the interactions at each step.
The partition function is usually defined as:

$$\mathbb{Z} = \sum e^{-\beta H} = \sum_{Spc} P(Spc), \tag{2}$$

where $P(Spc)$ can be thought of as an unnormalized probability distribution [60] over the spin configuration, Spc. Starting from the central pair on the lattice made up with q separate branches connecting each pair of spins, one follows only one of the branches of the tree out of q. This implies that $P(S_0, S'_{0'})$, i.e. $Spc = (S_0, S'_{0'})$, of a spin configuration with the spin value $(S_0, S'_{0'})$ at the central pair, can be written as:

$$P(S_0, S'_{0'}) = \exp\Big[\beta\big(J_3 S_0 S'_{0'} + h_1 S_0 + h_2 S'_{0'}\big)\Big]\Big[g_n(S_0, S'_{0'})\Big]^q, \tag{3}$$

$$P(\sigma_1, \sigma'_{1'}) = \exp\Big[\beta\big(J_4 \sigma_1 \sigma'_{1'} + D(\sigma_1^2 + \sigma_{1'}^{\prime 2}) + h_1 \sigma_1 + h_2 \sigma'_{1'}\big)\Big]\Big[g_{n-1}(\sigma_1, \sigma'_{1'})\Big]^q, \tag{4}$$

where,

$$g_n(S_0, S'_{0'}) = \sum_{\{\sigma_1, \sigma'_{1'}\}} \exp\Big[\beta\big(J_1 S_0 \sigma_1 + J_2 S'_{0'} \sigma'_{1'} + J_4 \sigma_1 \sigma'_{1'} + D(\sigma_1^2 + \sigma_{1'}^{\prime 2}) + h_1 \sigma_1 + h_2 \sigma'_{1'}\big)\Big]\Big[g_{n-1}(\sigma_1, \sigma'_{1'})\Big]^{q-1} \tag{5}$$

and

$$g_{n-1}(\sigma_1, \sigma'_{1'}) = \sum_{\{S_2, S'_{2'}\}} \exp\Big[\beta\big(J_1 S_2 \sigma_1 + J_2 S'_{2'} \sigma'_{1'} + J_3 S_2 S'_{2'} + h_1 S_2 + h_2 S'_{2'}\big)\Big]\Big[g_{n-2}(S_2, S'_{2'})\Big]^{q-1}. \tag{6}$$

In order to find the recursion relations, the following variables as ratios of the g_n functions for the spin-1/2 are introduced:

$$X_n = \frac{g_n(1/2, 1/2)}{g_n(-1/2, -1/2)},$$

$$Y_n = \frac{g_n(1/2, -1/2)}{g_n(-1/2, -1/2)},$$

$$Z_n = \frac{g_n(-1/2, 1/2)}{g_n(-1/2, -1/2)} \tag{7}$$

and for the spin-1, the g_{n-1} functions are considered:

$$\begin{aligned}
A_{n-1} &= \frac{g_{n-1}(1,1)}{g_{n-1}(0,0)}, \quad B_{n-1} = \frac{g_{n-1}(1,-1)}{g_{n-1}(0,0)}, \\
C_{n-1} &= \frac{g_{n-1}(1,0)}{g_{n-1}(0,0)}, \quad D_{n-1} = \frac{g_{n-1}(-1,1)}{g_{n-1}(0,0)}, \\
E_{n-1} &= \frac{g_{n-1}(-1,-1)}{g_{n-1}(0,0)}, \quad F_{n-1} = \frac{g_{n-1}(-1,0)}{g_{n-1}(0,0)}, \\
G_{n-1} &= \frac{g_{n-1}(0,1)}{g_{n-1}(0,0)}, \quad H_{n-1} = \frac{g_{n-1}(0,-1)}{g_{n-1}(0,0)}.
\end{aligned} \tag{8}$$

These variables are related to each other as follows:

$$\Delta_n = f(X_{n-2}, Y_{n-2}, Z_{n-2}), \tag{9}$$

$$\Theta_{n-1} = g(A_{n-3}, B_{n-3}, C_{n-3}, D_{n-3}, E_{n-3}, F_{n-3}, G_{n-3}, H_{n-3}), \tag{10}$$

where Δ and Θ refer to the three functions given in equation (7) and the eight functions given in equation (8), respectively. These functions are totally nonlinear; their explicit expressions are too long to be given here. Their numerical values are easily calculated by an iteration procedure. The initial choice of the recursion relations, i.e, the ratios of these functions, is completely arbitrary.
In the pairwise approach, both layers are partitioned into sublattices A and B. The sublattice magnetizations for layers G_1 and G_2 can be written as [58]:

$$\{M_{1,2}\} \longrightarrow \begin{array}{l} \{M_{1A}, M_{2A}\} \ for\ even\ n \\ \{M_{1B}, M_{2B}\} \ for\ odd\ n; \end{array} \tag{11}$$

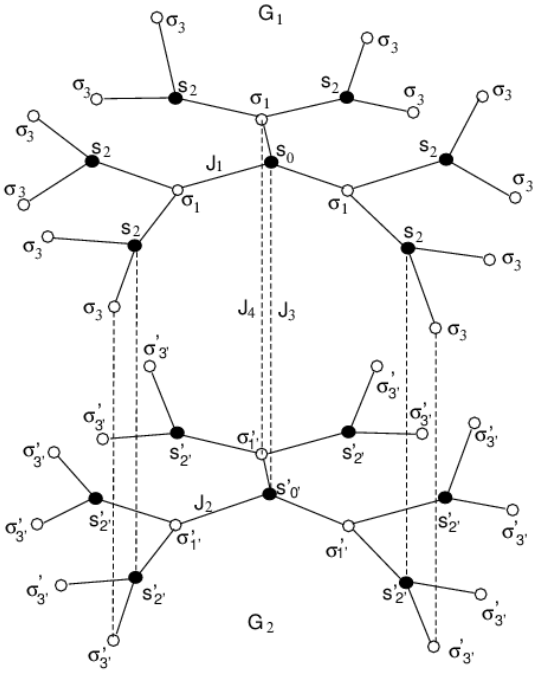

Figure 1. The bilayer Bethe lattice of coordination number $q = 3$. G_1 and G_2 refer to the upper and lower layers containing the spins labeled as (S_i, σ_i) and $(S'_{i'}, \sigma'_{i'})$, respectively. While J_1 and J_2 are the bilinear interaction parameters of spins in G_1 and G_2, J_3 and J_4 are those for the adjacent vertically aligned spins of G_1 and G_2.

the numbers 1 and 2 refer to the layers while A and B refer to the sublattices.
Similarly, the quadrupolar order-parameter Q can be written as:

$$\{Q_{1,2}\} \longrightarrow \begin{array}{l} \{Q_{1A}, Q_{2A}\} \ for \ even \ n \\ \{Q_{1B}, Q_{2B}\} \ for \ odd \ n, \end{array} \tag{12}$$

The free energy is obtained as;

$$\{F_n\} \longrightarrow \begin{array}{l} \{F_n^A\} \ for \ even \ n \\ \{F_n^B\} \ for \ odd \ n; \end{array} \tag{13}$$

then, the specific heat defined accordingly is:

$$\{C_n\} \longrightarrow \begin{array}{l} \{C_n^A\} \ for \ even \ n \\ \{C_n^B\} \ for \ odd \ n. \end{array} \tag{14}$$

Finally, the magnetic susceptibility is given by;

$$\{\chi_n\} \longrightarrow \begin{array}{l} \{(\chi_{1A})_n + (\chi_{2A})_n\} \ for \ even \ n \\ \{(\chi_{1B})_n + (\chi_{2B})_n\} \ for \ odd \ n. \end{array} \tag{15}$$

The sublattice magnetizations M_{1A}, M_{1B} and M_{2A}, M_{2B} of the layers G_1 and G_2 are defined as;

$$M_{1A} = \langle S \rangle \quad , \quad M_{1B} = \langle \sigma \rangle, \tag{16}$$

and

$$M_{2A} = \langle S' \rangle \quad , \quad M_{2B} = \langle \sigma' \rangle, \tag{17}$$

where $\langle ... \rangle$ denotes the usual thermal average. These quantities are calculated by means of the recursion relations as;

$$M_{1A} = \left[e^{\beta\left(0.25J_3+0.5(h_1+h_2)\right)} X_n^q + e^{\beta\left(-0.25J_3+0.5(h_1-h_2)\right)} Y_n^q - e^{\beta\left(-0.25J_3+0.5(-h_1+h_2)\right)} Z_n^q - e^{\beta\left(0.25J_3-0.5(h_1+h_2)\right)} \right] / 2\mathbb{Z}_A, \tag{18}$$

$$\begin{aligned} M_{1B} \ = \ & \left[e^{\beta(J_4+2D+h_1+h_2)} A_{n-1}^q + e^{\beta(-J_4+2D+h_1-h_2)} B_{n-1}^q + e^{\beta(D+h_1)} C_{n-1}^q \right. \\ & \left. - e^{\beta(-J_4+2D-h_1+h_2)} D_{n-1}^q - e^{\beta(J_4+2D-h_1-h_2)} E_{n-1}^q - e^{\beta(D-h_1)} F_{n-1}^q \right] / \mathbb{Z}_B \end{aligned} \tag{19}$$

and

$$M_{2A} = \Big[e^{\beta\left(0.25J_3+0.5(h_1+h_2)\right)}X_n^q - e^{\beta\left(-0.25J_3+0.5(h_1-h_2)\right)}Y_n^q + e^{\beta\left(-0.25J_3+0.5(-h_1+h_2)\right)}Z_n^q - e^{\beta\left(0.25J_3-0.5(h_1+h_2)\right)}\Big]/2\mathbb{Z}_A, \quad (20)$$

$$M_{2B} = \Big[e^{\beta(J_4+2D+h_1+h_2)}A_{n-1}^q - e^{\beta(-J_4+2D+h_1-h_2)}B_{n-1}^q + e^{\beta(-J_4+2D-h_1+h_2)}D_{n-1}^q - e^{\beta(J_4+2D-h_1-h_2)}E_{n-1}^q + e^{\beta(D+h_2)}G_{n-1}^q - e^{\beta(D-h_2)}H_{n-1}^q\Big]/\mathbb{Z}_B \quad (21)$$

where

$$\mathbb{Z}_A = e^{\beta\left(0.25J_3+0.5(h_1+h_2)\right)}X_n^q + e^{\beta\left(-0.25J_3+0.5(h_1-h_2)\right)}Y_n^q + e^{\beta\left(-0.25J_3+0.5(-h_1+h_2)\right)}Z_n^q + e^{\beta\left(0.25J_3-0.5(h_1+h_2)\right)}, \quad (22)$$

$$\mathbb{Z}_B = e^{\beta(J_4+2D+h_1+h_2)}A_{n-1}^q + e^{\beta(-J_4+2D+h_1-h_2)}B_{n-1}^q + e^{\beta(D+h_1)}C_{n-1}^q + e^{\beta(-J_4+2D-h_1+h_2)}D_{n-1}^q + e^{\beta(J_4+2D-h_1-h_2)}E_{n-1}^q + e^{\beta(D-h_1)}F_{n-1}^q + e^{\beta(D+h_2)}G_{n-1}^q + e^{\beta(D-h_2)}H_{n-1}^q + 1. \quad (23)$$

The layer magnetization and the total magnetization are defined as:

$$M_1 = \frac{1}{2}(M_{1A} + M_{1B}), \quad M_2 = \frac{1}{2}(M_{2A} + M_{2B}), \quad (24)$$

and

$$M_T = \frac{1}{2}(M_1 + M_2). \quad (25)$$

The order-parameter Q that is the quadrupole moment is defined as:

$$Q_{1B} = \langle\sigma^2\rangle; \quad Q_{2B} = \langle\sigma'^2\rangle \quad (26)$$

Since the spin-1/2 sublattices are the two-state and one order parameter systems, they have only M_{1A} and M_{2A} as the order parameters since Q_{1A} and Q_{2A} are constant and equal to 1/4. For the spin-1 sublattices, Q_{1B} and Q_{2B} have the following expressions:

$$Q_{1B} = \Big[e^{\beta(J_4+2D+h_1+h_2)}A_{n-1}^q + e^{\beta(-J_4+2D+h_1-h_2)}B_{n-1}^q + e^{\beta(D+h_1)}C_{n-1}^q + e^{\beta(-J_4+2D-h_1+h_2)}D_{n-1}^q + e^{\beta(J_4+2D-h_1-h_2)}E_{n-1}^q + e^{\beta(D-h_1)}F_{n-1}^q\Big]/\mathbb{Z}_B, \quad (27)$$

$$Q_{2B} = [e^{\beta(J_4+2D+h_1+h_2)}A_{n-1}^q + e^{\beta(-J_4+2D+h_1-h_2)}B_{n-1}^q + e^{\beta(-J_4+2D-h_1+h_2)}D_{n-1}^q + e^{\beta(J_4+2D-h_1-h_2)}E_{n-1}^q + e^{\beta(D+h_2)}G_{n-1}^q + e^{\beta(D-h_2)}H_{n-1}^q]/\mathbb{Z}_B. \quad (28)$$

Magnetic susceptibilities for layers G_1 and G_2 are given by:

$$\chi_1 = \lim_{h_1\to h}\frac{\partial M_1}{\partial h} \quad \text{and} \quad \chi_2 = \lim_{h_2\to h}\frac{\partial M_2}{\partial h}, \quad (29)$$

and the total susceptibility of the bilayer follows:

$$\chi_{Total} = \frac{1}{2}(\chi_1 + \chi_2). \quad (30)$$

Using the relation $F = -kT \log \mathbb{Z}$ and equations (7), (8), (22) and (23) in the thermodynamic limit ($n \to \infty$), one obtains the exact expression of the free energy in terms of the recursion relations. Thus, after some straightforward mathematical calculations, one finds:

$$-\beta F = \frac{1}{2-q} \log \mathbb{W}_1 - \frac{1-q}{2-q} \log \mathbb{W}_2 + \log \mathbb{Z}_A, \quad (31)$$

or

$$-\beta F = \frac{1}{2-q} \log \mathbb{W}_3 - \frac{1-q}{2-q} \log \mathbb{W}_1 + \log \mathbb{Z}_B, \quad (32)$$

where:

$$\begin{aligned} \mathbb{W}_1 &= e^{\beta(-0.5J_1-0.5J_2+J_4+2D+h_1+h_2)} A_{n-1}^{q-1} + e^{\beta(-0.5J_1+0.5J_2-J_4+2D+h_1-h_2)} B_{n-1}^{q-1} + e^{\beta(-0.5J_1+D+h_1)} C_{n-1}^{q-1} \\ &+ e^{\beta(0.5J_1-0.5J_2-J_4+2D-h_1+h_2)} D_{n-1}^{q-1} + e^{\beta(0.5J_1+0.5J_2+J_4+2D-h_1-h_2)} E_{n-1}^{q-1} + e^{\beta(0.5J_1+D-h_1)} F_{n-1}^{q-1} + e^{\beta(-0.5J_2+D+h_2)} G_{n-1}^{q-1} \\ &+ e^{\beta(0.5J_2+D-h_2)} H_{n-1}^{q-1} + 1, \end{aligned} \quad (33)$$

$$\mathbb{W}_2 = e^{\beta\left(0.25J_3+0.5(h_1+h_2)\right)} X_n^{q-1} + e^{\beta\left(-0.25J_3+0.5(h_1-h_2)\right)} Y_n^{q-1} + e^{\beta\left(-0.25J_3+0.5(-h_1+h_2)\right)} Z_n^{q-1} + e^{\beta\left(0.25J_3-0.5(h_1+h_2)\right)}, \quad (34)$$

$$\mathbb{W}_3 = e^{\beta\left(0.25J_3+0.5(h_1+h_2)\right)} X_{n-2}^{q-1} + e^{\beta\left(-0.25J_3+0.5(h_1-h_2)\right)} Y_{n-2}^{q-1} + e^{\beta\left(-0.25J_3+0.5(-h_1+h_2)\right)} Z_{n-2}^{q-1} + e^{\beta\left(0.25J_3-0.5(h_1+h_2)\right)}. \quad (35)$$

3. The phase diagrams

The temperature phase diagrams are obtained by studying the thermal variations of the order parameters, the response functions and the system free energy.

Let us point out that the results derived in the previous section are rather general. They are valid for the FM/FM ($J_1 > 0, J_2 > 0$), FM/AFM ($J_1 > 0, J_2 < 0$), AFM/FM ($J_1 < 0, J_2 > 0$), AFM/AFM ($J_1 < 0, J_2 < 0$) versions of the model. Here, we only restrict our study to the case: FM/FM and FM/AFM interactions. To reduce the number of model free parameters, all the interaction constants will be hereafter normalized with respect to the coupling parameter J_1.

3.1. The case of FM/FM interactions: $J_1 = J_2 = J > 0$

Let's start the investigation of the system in this case with the construction of some ground state (GS) phase diagrams. The zero temperature phase diagram is exactly calculated and may be useful to check the reliability of the theoretical results at low temperature. By means of the assumption that both layers are influenced by external opposite magnetic fields: $h_1 = -h_2 = h \geq 0$, the GS energies are obtained from Eq. 1 in units of J in rewriting this equation as follows:

$$\begin{aligned} \frac{E}{qJ} &= -\sum_{<plaq>} \Big[S_i\sigma_j + S'_{i'}\sigma'_{j'} + \frac{J_3}{qJ} S_i S'_{i'} \\ &+ \frac{J_4}{qJ}\sigma_j\sigma'_{j'} + \frac{D}{qJ}\left(\sigma_j^2 + \sigma_{j'}^{\prime 2}\right) \\ &+ \frac{h}{qJ}(S_i + \sigma_j - S'_{i'} - \sigma'_{j'})\Big]. \end{aligned} \quad (36)$$

In this expression, the summation is over the central plaquette that consists of four NN pairs of the two-layer system with one pair $< ij >$ from the layer G_1, one pair $< i'j' >$ from the layer G_2, and two pairs $< ii' >, < jj' >$ obtained by connecting the layers G_1 and G_2 between the

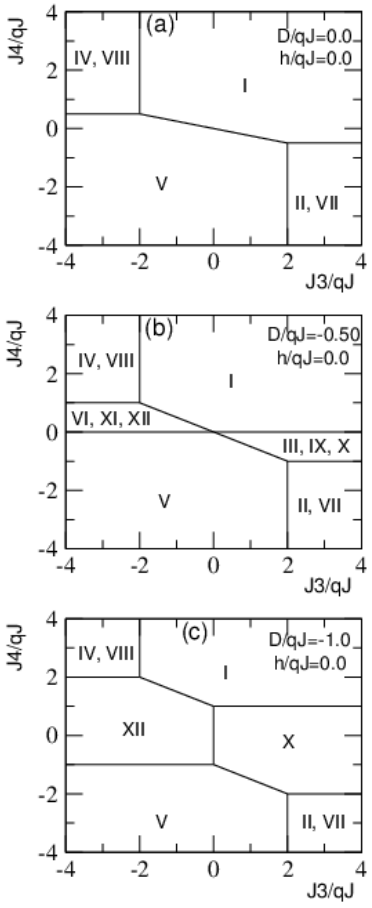

Figure 2. $T = 0$ phase diagrams of the mixed spin-1/2 and spin-1 Ising system on a bilayer Bethe lattice with FM/FM interactions on the $(J_3/qJ, J_4/qJ)$ plane for $h/qJ = 0$. Panel (a): $D/qJ = 0.0$; Panel (b): $D/qJ = -0.50$; Panel (c): $D/qJ = -1.0$.

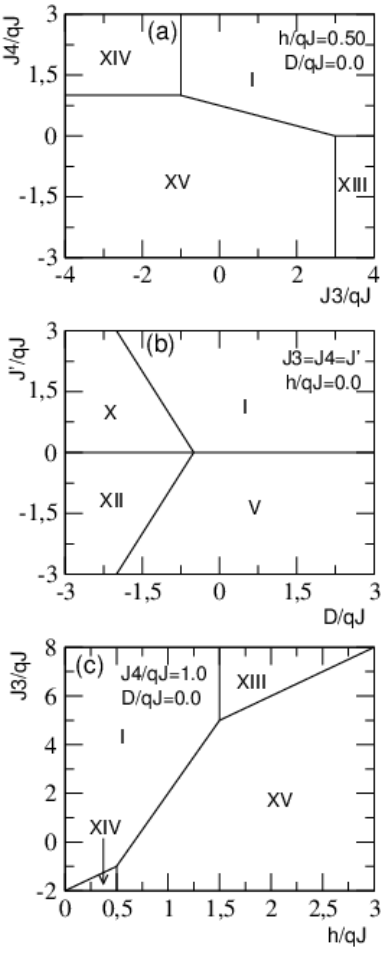

Figure 3. $T = 0$ phase diagrams of the mixed spin-1/2 and spin-1 Ising system on a bilayer Bethe lattice with FM/FM interactions. In the $(J_3/qJ, J_4/qJ)$ plane for $D/qJ = 0.0$ and $h/qJ = 0.50$ (a); in the $(D/qJ, J'/qJ)$ plane for $J_3 = J_4 = J'$ and $h/qJ = 0.0$ (b); in the $(h/qJ, J_3/qJ)$ plane for $J_4/qJ = 1.0$ and $D/qJ = 0.0$ (c).

only adjacent spins. The GS phase diagrams are calculated by comparing energies of different spin configurations. These equations are obtained for a general q. The Table 1 presents, for one plaquette the different types of GS configurations.

Phases I, III and IX correspond to the ferromagnetic ordering, i.e NN pairs are in the same ferro state.

Phases II, IV, VII, VIII, X, XIII and XIV correspond to the ferromagnetic ordering which is equivalent to the case where the GS of one layer is ferromagnetic and the GS of the other layer is antiferromagnetic phase, thus leading to the surface magnetic phase.

Phases V, VI, XI, XII and XV show ferromagnetic order in layers G_1 and G_2 separately. However the magnetizations on G_1 and G_2 are antiparallel, and these phases are called antiferromagnetic phases; the total magnetization of the bilayer system is zero.

Fig.2a is obtained on the $(J_3/qJ, J_4/qJ)$ plane for $D/qJ = h/qJ = 0$ and shows phases I, (II, VII), (IV, VIII), and V. The symmetry along the $J_3/qJ = 0$ and $J_4/qJ = 0$-axis is obvious. For further higher values of D/qJ when $h/qJ = 0.0$, the GS phase diagram remains qualitatively the same. When $D/qJ < 0$, (Figs.2b,c), additional configurations with lower spin values occur, i.e., zero values of spin-1 appear. For $h/qJ = 0.50$ and $D/qJ = 0$, (Fig.3a), the GS phase diagram is similar to that in Fig.2a with the replacement of phases (II, VII), (IV, VIII), and V by the phases XIII, XIV and XV respectively. Indeed, for $h/qJ > 0$ and $D/qJ = 0$, the GS phase diagram is similar to that in Fig.3a. The domain covered by the phase XV which has

Table 1. GS configurations. The phases are indicated with (s_0, σ_1) and $(s'_{0'}, \sigma'_{1'})$ NN pairs for the layers in G_1 and G_2 respectively, with the GS values of spin-1/2 and spin-1.

	$\pm 1/2$ ± 1		$\pm 1/2$ ± 1		$\pm 1/2$ ± 1		$\pm 1/2$ ± 1
I		II		III		IV	
	$\pm 1/2$ ± 1		$\pm 1/2$ ∓ 1		$\pm 1/2$ 0		$\mp 1/2$ ± 1
	$\pm 1/2$ ± 1		$\pm 1/2$ ± 1		$\pm 1/2$ ∓ 1		$\pm 1/2$ ∓ 1
V		VI		VII		VIII	
	$\mp 1/2$ ∓ 1		$\mp 1/2$ 0		$\pm 1/2$ ± 1		$\mp 1/2$ ∓ 1
	$\pm 1/2$ 0		$\pm 1/2$ 0		$\pm 1/2$ 0		$\pm 1/2$ 0
IX		X		XI		XII	
	$\pm 1/2$ ± 1		$\pm 1/2$ 0		$\mp 1/2$ ∓ 1		$\mp 1/2$ 0
	$\pm 1/2$ $+1$		$+1/2$ ± 1		$+1/2$ $+1$		
XIII		XIV		XV			
	$\pm 1/2$ -1		$-1/2$ ± 1		$-1/2$ -1		

zero magnetization, is extended by increasing the values h/qJ while those of phases I, XIII and XIV are reduced. So increasing values of h/qJ puts the system into the disordered configurations. Fig.3b is constructed on the $(D/qJ, J'/qJ)$ plane, where, only the phases I, V, X and XII are visible. When D is negative, as $|D|$ increases, states with lower spins are favoured; the zero value of spin-1 become persistent leaving the sublattices B with zero magnetization. It can be clearly seen from Fig.3c that as h/qJ becomes more and more higher, the area of phase XV increases.

Let us now analyze how thermal fluctuations disorder the previous GS phase diagrams. The temperature-dependent phase diagrams are constructed for low values of q by studying the thermal behaviours of the order parameters and the free energy. The two layers that are concerned are assumed to be influenced by external opposite magnetic fields: $h_1 = -h_2 = h \geq 0$. In the phase diagrams, the solid and dashed lines represent the second- (T_c-lines) and first-order (T_t-lines) phase transition lines respectively, and the triangles correspond to the positions of tricritical points where T_c-lines and T_t-lines meet.

In Fig.4, we show temperature-dependent phase diagrams for $q = 3-6$. For $q = 3, 4$, only T_c-lines are got whereas, for $q > 4$, T_t-lines appear with the existence of tricritical points. For $h/qJ = 0.5$, all transition lines, for different values of q, reach the $T = 0$-axis at the same value $J_4/J = 0$. Some phase diagrams show a reentrance (Figs.4a,b). For negative values of D/qJ, the phase boundaries present a wavy character (Fig.4d). In Fig.5, as the value of h/qJ increases, the transition lines moved to the higher J_4/J region. This behaviour is also detected for large negative values of D/qJ. Consequently, the region with nonzero magnetization is reduced.

The next four phase diagrams are displayed on several planes (Fig.6). The first one (Fig.6a) is calculated for $h/qJ = 0$ for $J_3/qJ = J_4/qJ = J'/qJ = 1.0$. In Figs.6a,b, one observes that the critical temperature monotonically decreases with decreasing values of J_3 and D, until it reaches zero. Figs.6c,d clearly indicate that an increase of h/J at fixed other parameters stabilize the ordered ferromagnetic phase. There, one also observes that an increase of the gap $\tilde{J} = |J_4 - J_3|$ shortens the T_t-lines when they exist. This implies that a critical gap $\tilde{J}_c(q)$ may exist for each value of q where T_t-lines may disappear! One remarks that the lower the q is, the lower the value of T_c will be at $h/J = 0$.

The last phase diagram (Fig.7) is obtained on the $(D/J, kT/J)$ plane when both interlayer interaction parameters are set to zero. This phase diagram is similar to the one obtained in Fig.6a.

We have found two topological types of phase diagrams:

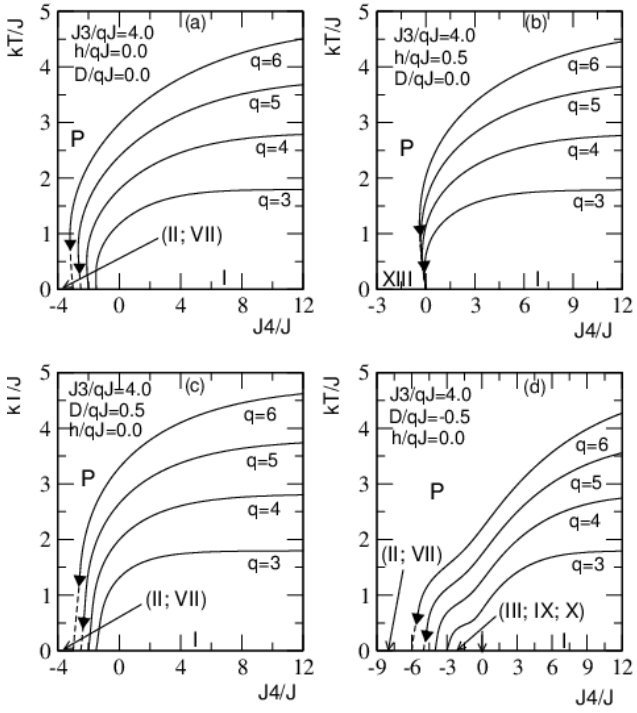

Figure 4. Temperature phase diagrams of the model for $q = 3, 4, 5$ and 6 in the $(J_4/J, kT/J)$ plane when $J_1 = J_2 = J > 0$ and $J_3/qJ = 4.0$. The solid and dashed lines correspond to the second-order and the first-order phase transition lines respectively. Tricritical points are indicated with filled triangles. Panel (a): $h/qJ = 0.0$ and $D/qJ = 0.0$; panel (b): $h/qJ = 0.5$ and $D/qJ = 0.0$; panel (c): $h/qJ = 0.0$ and $D/qJ = 0.5$; panel (d): $h/qJ = 0.0$ and $D/qJ = -0.5$.

diagrams where all transitions lines are T_c-lines (for $q \leq 4$) and diagrams with T_c-lines and T_t-lines with triciritcal points ($q > 4$). So increasing the coordination number q does display qualitative changes in the diagrams. This can be understood as follows. The Bethe lattice approximation is a kind of mean-field calculation. When the coordination number q increases, the value of the effective field of the neighbouring spins that acts on a giving spin becomes more or less important. This may induce changes in the nature of the phase boundaries.

Since J_3 and J_4 are the bilinear interlayer interaction constants between the layers G_1 and G_2, when both are equal to zero the two-layer Bethe lattice reduces to two identical independent one-layer Bethe lattices with mixed spin-1/2 and spin-1. Let us point out that if $\tilde{J} = 0$ in the present system (see Figs.6a, 7), one gets results that are consistent with those in Refs. [12, 50].

3.2. The case of FM/AFM interactions: $J_1 > 0$ and $J_2 < 0$

Let us first show how the NN interactions affect the total magnetization. We only illustrate the case $q = 3$ due to similarities with other cases. We used the extended Néel classification [1, 61] to refer to different types of temperature dependence of the total magnetization. The thermal variation of the total magnetization has been found to be of Q-, R-, N-, S-, L- and P-type (Fig.8).

Monotonic decrease of the magnetization with increasing temperature indicates Q- and R-type behaviours. The Q-type always displays a steep decrease close to the Néel temperature T_N. The latter shows an intermediate relatively rapid decrease regime before an abrupt decay to zero at T_N. Another familiar N-type curve is characterized by one compensation point at which the resultant magnetization vanishes due to a complete cancellation of the bilayer magnetization. The stair-like S-shaped dependence initially exhibits a steep decrease of the magnetization that almost completely diminishes in the intermediate temperature regime and finally, a second steep decrease

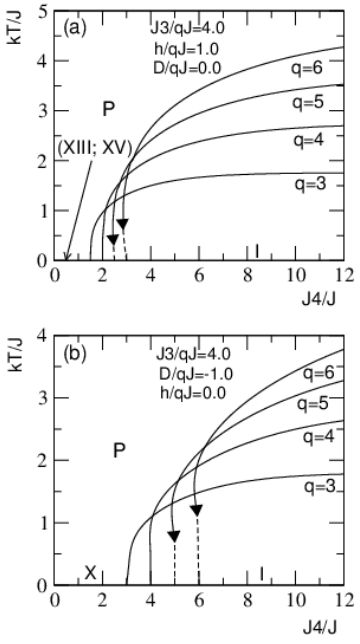

Figure 5. Temperature phase diagrams of the model for $q = 3, 4, 5$ and 6 in the $(J_4/J, kT/J)$ plane when $J_1 = J_2 = J > 0$ and $J_3/qJ = 4.0$. The solid and dashed lines correspond to the second-order and the first-order phase transition lines respectively. Tricritical points are indicated with filled triangles. Panel (a): $h/qJ = 1.0$ and $D/qJ = 0.0$; panel (b): $D/qJ = -1.0$ and $h/qJ = 0.0$.

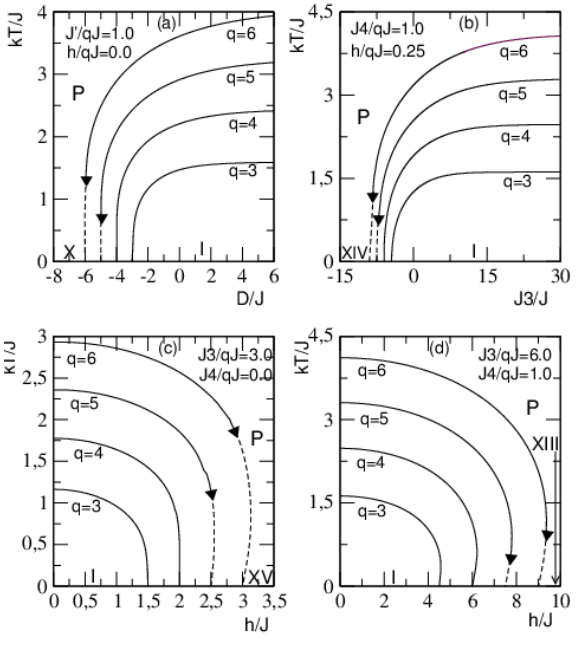

Figure 6. Temperature phase diagrams of the model for $q = 3, 4, 5$ and 6 when $J_1 = J_2 = J > 0$. The solid and dashed lines correspond to the second-order and the first-order phase transition lines, respectively, and the tricritical points are indicated with filled triangles. In the $(D/J, kT/J)$ plane for $J_3/qJ = J_4/qJ = J'/qJ = 1.0$ and $h/qJ = 0.0$ (a); in the $(J_3/J, kT/J)$ plane for $J_3/qJ = 1.0$, $h/qJ = 0.25$ and $D/qJ = 0.0$ (b); in the $(h/J, kT/J)$ for $J_3/qJ = 3.0$, $J_4/qJ = 0.0$ and $D/qJ = 0.0$ (c); in the $(h/J, kT/J)$ for $J_3/qJ = 6.0$, $J_4/qJ = 1.0$ and $D/qJ = 0.0$ (d).

follows near the critical temperature. The L-type and P-type curves are very analogous, displaying a temperature-induced maximum as the temperature is raised from zero. However, for the L-type curve [62], the resultant magnetization starts from zero [63]. These morphologies depend strongly on the values of the interaction parameters of the model.

We have also studied the effect of the interlayer bilinear exchange interaction parameters on the critical temperature of the bilayer system in the absence of other constraints, in particular for $J_2/J_1 = -1.50$. Our results for the transition temperature as a function of J_3/J_1 and J_4/J_1 are shown in Fig.9.

The temperature-dependent phase diagrams are obtained for $q = 3, 4$ and 6 and their phase transition lines are labeled with gray solid, dashed and black solid lines, respectively. The arrows indicate the phase separation points according to the GS phase diagrams. Two ground state (GS) configurations are found for the central plaquette deep inside the two-layer Bethe lattice as indicated in Table 1: Phases II and IV are the surface FM phases, i.e. layers G_1 and G_2 are FM and AFM types, respectively.

The first phase diagram of the model is obtained on the $(J_4/J_1, kT/J_1)$ plane. As seen in Fig.9a, for $J_3/qJ_1 = 1.0$, the critical lines (T_N-lines) start from constant temperatures at higher negative values of J_4/J_1. The wing-shaped second-order lines, i.e. T_N-lines, are seen at higher temperatures for higher q and separate the ordered phases II, and IV from the paramagnetic (P) phase. The left wings are seen at temperature higher than for the right ones, since situation where $J_1 > 0$, $J_2 < 0$, $J_3 > 0$ and $J_4 < 0$ favours the surface FM phase II but for $J_1 > 0$, $J_2 < 0$, the surface FM phase is favoured whereas the case $J_3 > 0$ and $J_4 > 0$ favours the FM phase, so the phase II is more resistive to temperature than the phase IV. The T_N-lines do not reach the $T = 0$-axis since both phases II and IV are the surface FM phases. These results bear some resemblance with those reported in Ref. [58] for the two-layer spin-1/2 Ising model. When $J_3/qJ_1 = -1.0$, one obtains the mirror image of Fig.9a (see Fig.9b). In Fig.9c, the roles of J_3 and J_4 are exchanged. One observes here that the critical temperature exhibits a smooth monotonic decline with increasing values of J_3/J_1 and becomes constant at large positive values. This phase diagram is qualita-

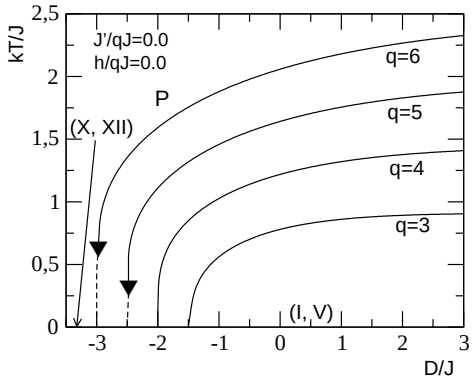

Figure 7. Temperature phase boundaries of the model for $q = 3, 4, 5$ and 6 in the $(D/J, kT/J)$ plane when $J_1 = J_2 = J > 0$ and $J_3/qJ = J_4/qJ = J'/qJ = 0.0$. The solid and dashed lines correspond to the second-order and the first-order phase transition lines respectively. Tricritical points are indicated with filled triangles.

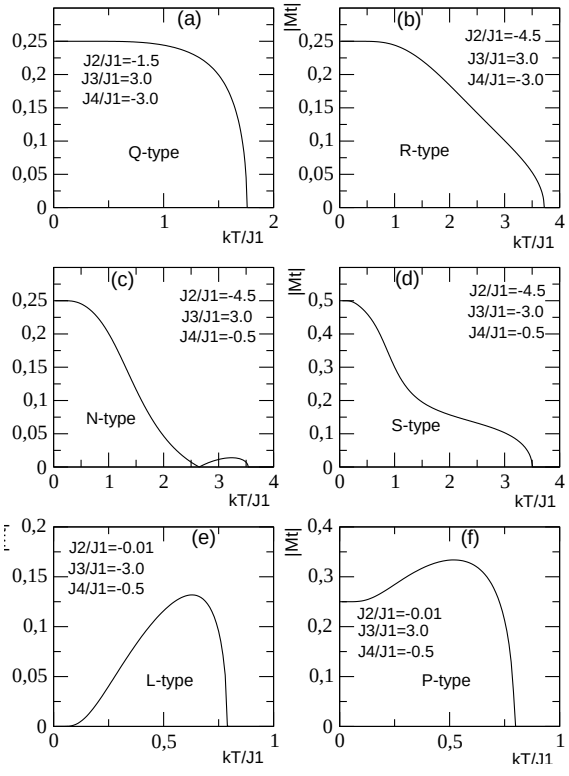

Figure 8. The temperature variation of the resultant magnetization of the model for $q = 3$. Values considered for the model parameters are indicated in different panels.

tively similar to the one displayed in Fig.3b of Ref. [58].

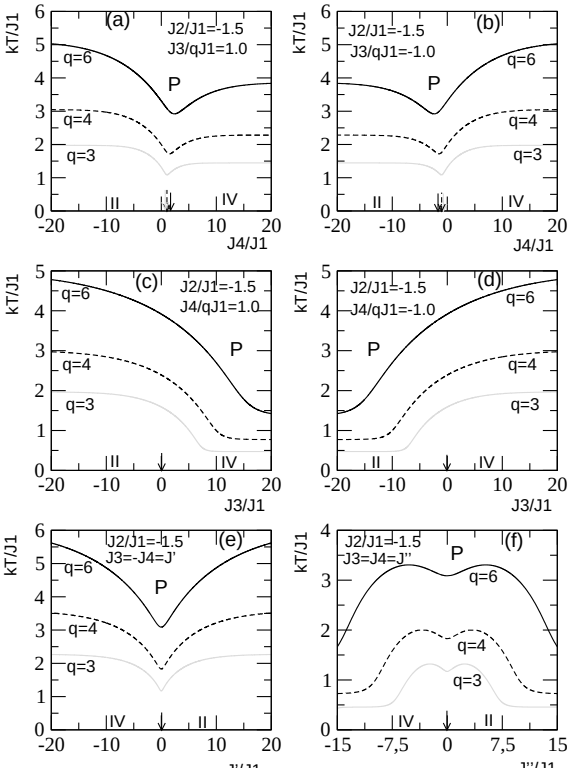

Figure 9. Temperature phase diagrams of the model are presented for $q = 3, 4$, and 6 when $J_2/J_1 = -1.5$, $D/qJ = 0.0$ and $h/qJ = 0.0$. Corresponding transition lines are labeled with gray solid, dashed and black solid lines, respectively; on the $(J_4/J_1, kT/J_1)$ plane for $J_3/qJ_1 = 1.0$ (a) and $J_3/qJ_1 = -1.0$ (b); on the $(J_3/J_1, kT/J_1)$ plane for $J_4/qJ_1 = 1.0$ (c) and $J_4/qJ_1 = -1.0$ (d); on the $(J'/J_1, kT/J_1)$ for $J_3 = -J_4 = J'$ (e) and on the $(J''/J_1, kT/J_1)$ for $J_3 = J_4 = J''$ (f).

The mirror image of Fig.9c is obtained for $J_4/qJ_1 = -1.0$ (see Fig.9d). Fig.9e is obtained on the $(J'/J_1, kT/J_1)$ plane for $J_3 = -J_4 = J'$, where the T_N's are constant at large and negative values of J'/J_1. This happens also at large and positive values of J'/J_1. The T_N-lines present concavities at about $J'/J_1 = 0.0$ for all values of q. The critical temperatures are the same for large negative or positive values of J'/J_1 since the case $J_1 > 0$, $J_2 < 0$ and $J' < 0$ favours the surface FM phase IV. For $J_1 > 0$, $J_2 < 0$ and $J' > 0$, the surface FM phase II is favoured. This phase diagram is qualitatively similar to those reported on the spin-3/2 Ising model AFM/AFM two-layer lattice with crystal field in Fig.3 of Ref. [57]. Fig.9f is obtained for $J_3 = J_4 = J''$ on the $(J''/J_1, kT/J_1)$ plane. The T_N-lines are horizontal at large and negative values of J''/J_1, but as J''/J_1 increases, the critical temperature increase continuously and reach a maximum. As J''/J_1 is raised further, the T_N's decrease and show a minimum for all q at about $J''/J_1 = 0.0$. The same behaviour is obtained for

positive values of J''/J_1. This phase diagram is symmetric with respect to J''/J_1. Moreover, when the roles of J_1 and J_2 are exchanged and $J_1/|J_2| = 1.5$, the phase diagrams on the $(J_4/|J_2|, kT/|J_2|)$, $(J_3/|J_2|, kT/|J_2|)$, $(J'/|J_2|, kT/|J_2|)$, and $(J''/|J_2|, kT/|J_2|)$ planes for respectively $J_3/q|J_2| = \pm 1$, $J_4/q|J_2| = \pm 1$, $J_3 = -J_4 = J'$ and $J_3 = J_4 = J''$ are respectively the same when compared to those displayed in Fig.9.

4. Conclusion

We have studied a bilayer mixed spin Ising system in terms of interlayer and intralayer coupling constants in the presence of crystal field and external magnetic field constraints. The $T = 0$-behaviours of the system are investigated through some ground state phase diagrams relying on energies of possible spin configurations of the system. Numerical solutions of the recursion relations enabled us to study the thermal behaviours of the order parameters and the system free energy. Interesting behaviours such as the existence of the first-order and second order transitions as well as compensation point are found. The first order transition occurs for coordination number $q > 4$. Topologically different phase diagrams are found by tuning values of the coupling constants. Sometimes, tricritical points and also reentrant phase diagrams are observed. When the nearest-neighbour coupling constants are fixed, the external magnetic fields influence the system by shortening the first order transition lines. Increasing negative values of the crystal field stabilizes the disordered phase.

The existence of compensation points has been reported in many previous works on mixed-spin Ising models [51, 56, 59, 63]. It has a technological interest since this property is used in several devices for information storage and retrieval. The different results achieved here bear some resemblances with those reported in Refs. [12, 50, 57, 58]. The present model can be extended to study spin transitions in spin-crossover materials. Then some coupling constants may depend on the temperature or the ligand-field strength. Work on this subject is in progres and preliminary results look fascinating.

References

[1] L. Néel, Ann. Phys. 3, 137 (1948)

[2] D. Gatteshi, O. Khan, J. S. Miller, F. Palacio (Eds.), Magnetic Molecular Materials, In: NATO ASI Series (Kluwer Academic, Dordrecht, 1991)

[3] O. Khan, Molecular Magnetism (VCH Publishers, New York, 1993)

[4] O. Kahn, in: E. Coronado, et al. (Eds.), Molecular Magnetism: From Molecular Assemblies to the Devices, (Kluwer Academic Publishers, Dordrecht, 1996)

[5] S. L. Schofield, R. G. Bowers, J. Phys. A 13, 3697 (1980)

[6] N. Benayad, J. Zittartz, Z. Phys. B 81, 107 (1990)

[7] B. Boechat, R. A. Filgueiras, L. Marins, C. Cordeiro, N. S. Branco, Mod. Phys. Lett. B 14, 749 (2000)

[8] B. Boechat, R. A. Filgueiras, C. Cordeiro, N. S. Branco, Physica A 304, 429 (2002)

[9] S. L. Schofield, R. G. Bower, J. Phys. A Math. Gen. 14, 2163 (1981)

[10] B. Y. Yousif, R. G. Bower, J. Phys. A Math. Gen. 17, 3389 (1984)

[11] F. K. Tang, J. Phys. A 21, L1097 (1988)

[12] E. Albayrak, M. Keskin, J. Magn. Magn. Mater. 261, 196 (2003)

[13] T. Iwashita, N. Uryu, Phys. Lett. A 96, 311 (1983)

[14] T. Iwashita, N. Uryu, J. Phys. Soc. Jpn. 53, 721 (1984)

[15] T. Iwashita, N. Uryu, Phys. Stat. Sol. (b) 125, 551 (1984)

[16] T. Kaneyoshi, Phys. Rev. B 34, 7866 (1986)

[17] T. Kaneyoshi, J. Phys. Soc. Jpn. 56, 2675 (1987)

[18] T. Kaneyoshi, J. Phys. Soc. Jpn. 58, 1755 (1989)

[19] T. Kaneyoshi, J. Magn. Magn. Mater. 98, 201 (2000)

[20] A. L. De Lima, B. D. Stošić, I. F. Fittipaldi, J. Magn. Magn. Mater. 226-230, 635 (2001)

[21] T. Kaneyoshi, Solid State Commun. 70, 975 (1989)

[22] T. Kaneyoshi, E. F. Sarmento, I. F. Fittipaldi, Phys. Stat. Sol. (B) 150, 261 (1988)

[23] J. A. Plascak, Physica A 198, 655 (1993)

[24] T. Kaneyoshi, J. C. Chen, J. Magn. Magn. Mater. 98, 201 (1991)

[25] N. Benayad, A. Klümper, J. Zittartz, A. Benyoussef, Z. Phys. B Condens. Matter 77, 333 (1989)

[26] G. M. Zhang, C. Z. Yang, Phys. Rev. B 48, 9452 (1993)

[27] G. M. Buendia, M. A. Novotny, J. Zhang, In: D. P. Landau, K. K. Mon, H. B. Schüttler (Eds.) Computer Simulations in Condensed Matter Physics VII (Springer Proceeds in Physics 78, Springer, Heidelberg, 1994) 223

[28] G. M. Buendia, M. A. Novotny, J. Phys. Condens. Matter 9, 5951 (1997)

[29] H. F. V. De Resende, F. C. Sa Barreto, J. A. Plascak, Physica A 149, 606 (1988)

[30] J. W. Tucker, J. Magn. Magn. Mater. 195, 733 (1999)

[31] H. J. Elmers, Int. J. Mod. Phys. B 9, 3115 (1995)

[32] U. Bovensiepen et al., Phys. Rev. Lett. 81, 2368 (1998)

[33] H. Matsuyama, C. Haginoya, K. Koike, Phys. Rev. Lett. 85, 646 (2000)

[34] H. Ohldag, A. Scholl, F. Nolting, S. Anders, F. U. Hillebrecht, J. Stohr, Phys. Rev. Lett. 86, 2878 (2001)
[35] G. Chern, L. Horng, W. K. Shieh, T. C. Wu, Phys. Rev. B 63, 94421 (2001)
[36] Y. Ijiri, J. A. Borchers, R. W. Erwin, S.-H. Lee, P. J. van der Zaag, R. M. Wolf, Phys. Rev. Lett. 80, 608 (1998)
[37] An Du, Yan Ma, Zeng-hui Wu, J. Magn. Magn. Mater. 305, 233 (2006)
[38] M. N. Baibich et al., Phys. Rev. Lett. 61, 2472 (1988)
[39] G. Binasch, P. Grunberg, F. Saurenbach, W. Zinn, Phys. Rev. B 39, 4828 (1989)
[40] R. Wu, A. J. Freeman , Phys. Rev. B 45, 7205 (1992)
[41] M. Donath, J. Phys.: Condens. Matter 11, 9421 (1999)
[42] Digest 13-th Int. Colloq. on Magnetic Films and Surfaces, Glasgow, (1991)
[43] Z. B. Li, Z. Shuai, Q. Wang, H. J. Luo, L. Schülke, J. Phys. A Math. Gen. 34, 6069 (2001)
[44] A. M. Ferrenberg, D. P. Landau, J. Appl. Phys. 70, 6215 (1991)
[45] J. Oitmaa, I. G. Enting, J. Phys. A Math. Gen. 8, 1097 (1975)
[46] A. Lipowski, Physica A 250, 373 (1998)
[47] M. Kurota, R. Kikuchi, T. Watari, J. Chem. Phys. 21, 434 (1953)
[48] C. Domb, Adv. Phys. 9, 208 (1960)
[49] N. Sh. Izmailian, C.-K. Hu, Physica A 254, 198 (1998)
[50] N. R. da Silva, S. R. Salinas, Phys. Rev. B 44, 852 (1991)
[51] R. A. Yessoufou, S. Bekhechi, F. Hontinfinde, Eur. Phys. J. B 81, 137 (2011) and references therein.
[52] J. Kple, R. A. Yessoufou, F. Hontinfinde, Afr. Rev. Phys. 7, 319 (2012) and references therein.
[53] C.-K. Hu, N. Sh. Izmailian, K. B. Oganesyan, Phys. Rev. E 59, 6489 (1999)
[54] E. Albayrak, O. Canko, Physica A 373, 363 (2007)
[55] O. Canko, E. Albayrak, Phys. Rev. E 75, 011116 (2007)
[56] E. Albayrak, S. Yilmaz, Physica A 387, 1173 (2008)
[57] E. Albayrak, A. Yigit, Chin. Phys. B. 18, 4193 (2009)
[58] E. Albayrak, A. Yigit, Acta Physica Polonica A 116, 127 (2009)
[59] K. Htoutou, A. Ainane, M. Saber, J. Magn. Magn. Mater. 269, 245 (2004)
[60] E. Albayrak, S. Yilmaz, S. Akkaya, Physica A 381, 189 (2007)
[61] S. Chikazumi, Physics of Ferromagnetism (Oxford University Press, Oxford, 1997)
[62] B. Barbara, D. Gignoux, C. Vettier, Lectures on Modern Magnetism (Springer, Berlin, 1988)
[63] J. Strečka, Physica A 360, 379 (2006)